RESEARCH ARTICLE

NANO · MICRO small
www.small-journal.com

Reaction-Driven Migration Dynamics of Nano-Metal Particles Unraveled by Quantitative Electron Microscopies

Bing Zhao, Fan Zhang, Deyang Gao, Gang Meng, Hua Li, Wei Liu, and Mao Ye**

The stability of supported nano-metal catalysts holds significant importance in both scientific and economic practice, beyond the long pursuit of enhanced activity. While previous efforts have concentrated on augmenting the interaction between nano-metals and carriers, in the thermodynamic macro-perspective, to achieve optimized repression upon particle migration coalescence and Ostwald ripening, nevertheless, the microscale kinetics of migrating catalyst particles driven by the reaction remains unknown. In this work, the migration of nano-copper particles is investigated during hydrogen oxidation reaction by utilizing high spatiotemporal resolution of environmental transmission electron microscopy. It is shown that there exists a delicate correlation between the migration dynamics of nano-copper particles and the evolution of asymmetrically distributed Cu and Cu_2O phases over the particle surface. It is found that the interplay of reduction and oxidation near the surface areas filled with Cu and Cu_2O phases can facilitate the pressure gradient, which drives the migration of nano-particles. A driving force model is therefore established which is capable of qualitatively explaining the influences of reaction conditions such as temperature and hydrogen-to-oxygen ratio on the reaction-driven particle migration. This work adds a potential yet critical perspective to understanding particle migration and thus the nano-metal catalyst particle sintering in heterogeneous catalysis.

1. Introduction

Metal-supported catalysts play a pivotal role in the chemical industry[1] facilitating the production of basic chemicals via a wide variety of processes, such as naphtha reforming, water-gas shifting,[2] methanation,[3] ammonia synthesis, and among many others.[4] Metal catalysts, in particular the nano-sized metal particles, are challenged by the deactivation and active surface diminishment due to particle sintering at elevated temperatures.[5,6] Understanding the mechanisms underlying nano-metal particle sintering, however, remains a non-trivial task for heterogeneous catalysis.[7,8]

So far two mechanisms underlying nano-metal particle sintering, i.e., Ostwald ripening (OR)[9] and particle migration and coalescence (PMC),[10] have been identified. The OR mechanism is related to the inter diffusion of metal atoms or molecular species and attracts a wealth of research.[11–15] Meanwhile, the studies on PMC are relatively scarce. It is found that the primary approach for retarding the migration of particles involves strengthening the interaction between metal and corresponding carriers.[16] A variety of sinter-resistant catalysts have been developed following various approaches. Several strategies, such as strong metal support interactions (SMSI),[17,18] spatial confinement, and geometric shielding by embedding nanoparticles within zeolite channels, metal-organic frameworks, and encapsulating nanoparticles in thin films, have been proposed in real practice. However, the intrinsic reasons dominating the migration and coalescence of metal particles, which directly trigger particle sintering in the aforementioned approaches, have not been fully understood. Research related to migration dynamics has primarily focused on charge, metal ions, or grain boundaries.

A theoretical study by Hu et al. revealed that there is a critical inter-particle distance notably impeding the metal catalyst sintering.[19] They showed that the proper interaction strength between metal and carriers is critical for leveraging the balance between the migration behavior of nano-metals and the transformation of individual atoms, facilitating the synthesis of high-performance catalysts.[20] Experimental studies, in particular in situ characterizations, have manifested that the metal catalysts could undergo substantial changes during the reaction process, and their shape, size, and velocity would change markedly from their initial to final states.[21,22] Recently Huang et al.[23] found that nano-copper particles demonstrate the oscillatory motion in the redox reaction, which is closely relevant to the mutual diffusion between Cu and Cu_2O phases on the particle surface.[24] They proposed that the change in the

B. Zhao, G. Meng, M. Ye
Department of Chemical Physics
University of Science and Technology of China
Hefei, Anhui 230026, China
E-mail: maoye@dicp.ac.cn

B. Zhao, F. Zhang, D. Gao, H. Li, W. Liu, M. Ye
Dalian Institute of Chemical Physics
Chinese Academy of Sciences
Dalian, Liaoning 116023, China
E-mail: lihua@dicp.ac.cn

F. Zhang, W. Liu, M. Ye
University of Chinese Academy of Sciences
Beijing 100049, China

The ORCID identification number(s) for the author(s) of this article can be found under https://doi.org/10.1002/smll.202405759

DOI: 10.1002/smll.202405759

surface structure of nano-metal particles might be induced by the interaction between metal particles and chemical reaction gases.[25–28] However, a detailed analysis of the driving force controlling the motion and thus migration of nano-metal particles, is still absent. Since Ruska's groundbreaking utilization of environmental transmission electron microscopy (ETEM) to investigate gas-solid interactions,[29] in situ/*operando* TEM has been commonly used in capturing and documenting catalyst particle deformation,[30] fragmentation, sintering,[31] and interactions involving strong metal alloys[32] and metal supports.[33] Meanwhile, in situ, TEM has played a crucial role in various research areas. For example, it has been instrumental in understanding the applications of nanostructured materials in novel devices,[34–36] studying the growth dynamics of nanocrystals,[37,38] and exploring the interactions between nanocrystals and other material interfaces.[39] In these studies, in situ TEM demonstrates its powerful real-time imaging capabilities at the atomic scale, both spatially and temporally. In this work we used ETEM to study the migration dynamics of nano-copper particles under hydrogen oxidation reaction, intending to directly unveil the driving force for the migration of nano-metal particles in heterogeneous catalytic processes. It is shown that the high spatio-temporal resolved migration behaviors of metal nanoparticles can be tracked using in situ ETEM and a driving force model can be established to illustrate the intricate interplay between migration dynamics and reaction-driven micro-structure evolution in heterogeneous catalysis.

2. Results and Discussion

2.1. Particle Migration Analysis and Driving Force Model Development

The morphological and surface phase changes of nano-copper particles during hydrogen oxidation have been examined with High-Resolution Transmission Electron Microscopy (HRTEM) (**Figure 1**). Three characteristic crystal planes, that is Cu (200), Cu (111), and Cu_2O (220), are revealed, confirming the coexistence of both metal and oxide phases on the surface of individual migrating particles (Figures 1b–d). Distribution of Cu and Cu_2O phases can be obtained through inverse fast Fourier transform (IFFT) about the diffraction spots of these two phases. The typical distribution of Cu and Cu_2O phases on the surface of catalytic particles, as illustrated in Figures 1e–h, coincides with the results reported by Huang et al.[23] Asymmetric distribution is present even before the particles begin to migrate. During the catalytic reaction, an uneven distribution of Cu and Cu_2O phases gradually forms on the surface of the Cu particles (Figures S1c–e, Supporting Information), implying that there might be an intrinsic correlation between the asymmetric distribution of Cu and Cu_2O and the particle migration. As the chemical reaction proceeds, this uneven distribution would lead to non-uniform gas pressure on the particle surface. We define the uneven distribution of Cu and Cu_2O as shown in Figure 1h, or the concentrated distribution of Cu and Cu_2O on opposite sides of the particle surface along the migration direction as shown in Figure 1i, as the asymmetric distribution. A distinctive trend, as observed, is that Cu tends to accumulate along the particle migration direction accompanied by a reduction of Cu_2O during the migration process (Figure 1i; Figure S1b, Supporting Information).

To further unveil the underlying physics, we focus on the micro-scale analysis of the reactions near the surface, as shown in Figure 1j. As can be seen, two main reactions will occur. One is the oxidation reaction which will occur near the surface of the nanoparticles filled with the Cu phase:

$$4Cu + O_2(g) \xrightarrow{k_1} 2Cu_2O \tag{1}$$

Another is the reduction reaction of Cu_2O that will take place near the surface filled with Cu_2O phase:

$$Cu_2O + H_2(g) \xrightarrow{k_2} 2Cu + H_2O(g) \tag{2}$$

Note that the oxidation reaction shown in Equation (1) is a typical gas molar number reduction reaction, which results in the change of gas pressure from P_0 to P_1. Meanwhile, the reduction reaction shown in Equation (2) is a constant gas molar number reaction, and thus the gas pressure P_0 will remain unchanged. The asymmetric distribution of Cu and Cu_2O on the surface of the nanoparticle, therefore, will lead to the pressure gradient around the nanoparticle. The force imposed on the nanoparticle can be represented as the integration of gas pressure over the entire particle surface (see Equation (3)):

$$F = -\int P\vec{n}dS \tag{3}$$

This driving force appears as soon as the reaction starts, which will induce the migration of nanoparticles. Further, we can reformulate the driving force (see Equation (4)) based on a detailed analysis (see the Supporting Information), which can distinctly elucidate the factors influencing the driving force during the particle migration.

$$\int_0^{\Delta t} \vec{F}dt = -RT\Delta t^2 k_1 \overline{c_{O_2}} \int \overline{c_{Cu}}\,\vec{n}\,dS \tag{4}$$

These factors include the reaction temperature T, the reaction rate constant k_1, the concentration of oxygen c_{O2}, and the concentration of Cu phase c_{Cu}. Equation (4) shows that the driving force and thus the migration velocity of copper nanoparticles, is closely linked to the consumption rate of oxygen γ_{O2}. We further assumed that, at the equilibrium state, the consumption rate of O_2 equals that of H_2. Any hindrances of either the oxidation or reduction reaction will lead to the change of driving force and result in the fluctuation of the migration motion of nanoparticles.

2.2. Statistics of the Fractions of Cu and Cu_2O Phases on Nano-Particle Surface

During particle migration, both oxidation and reduction reactions occur and compete. This will lead to the continuous change of both the metal and oxidate phases over the surface of nanoparticles throughout the reaction process. We examined the evolution of phase distribution over multiple particles during the reaction process using selected area electron diffraction (SAED).[40,41]

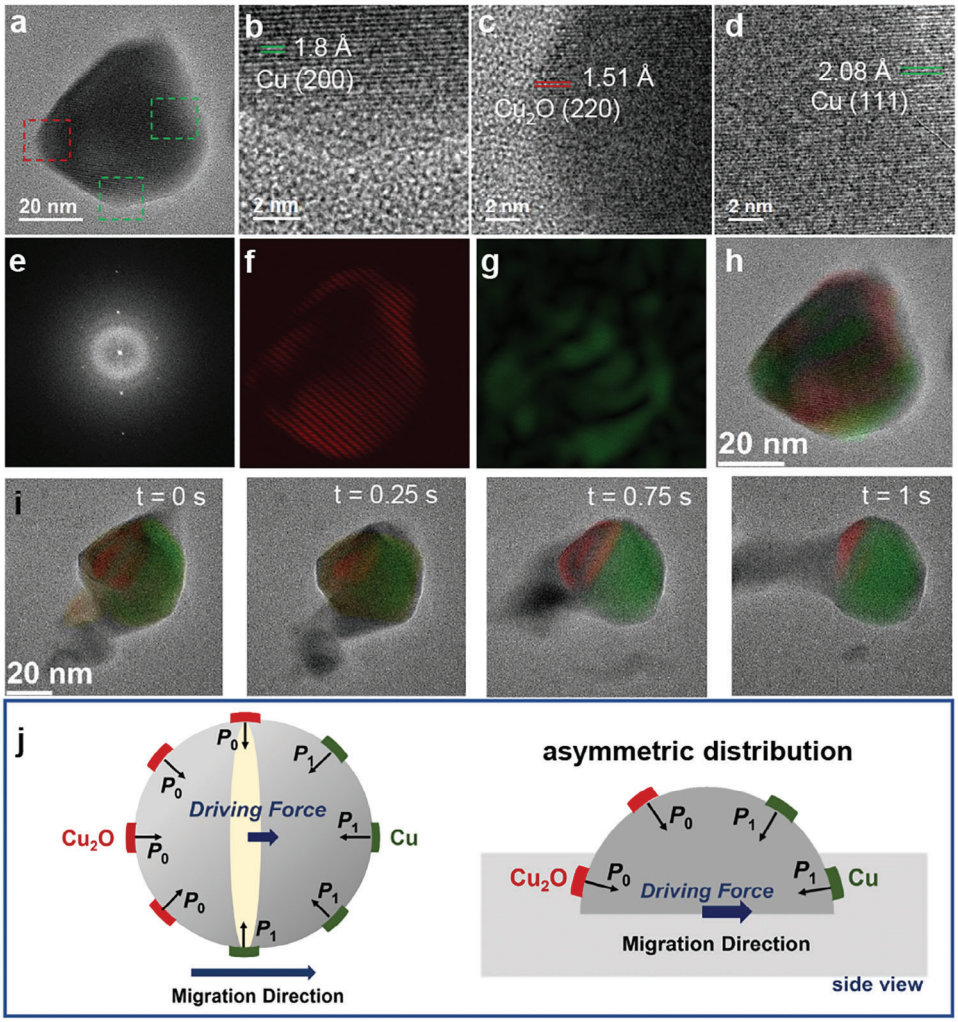

Figure 1. Micro-structure and phase evolution on the surface of migrating Cu particles. a–d) TEM images of a nano-copper particle and enlarged HRTEM images from the regions indicated by the red and green dashed rectangles. e–h) The phase distribution of Cu (green) and Cu_2O (red) on a catalytic particle obtained through inverse fast Fourier transform (IFFT) analysis. i) Dynamic evolved elemental mapping of a migrating Cu particle. j) Images depicting the mechanism of the particle migration.

Figure 2a,b display the SAED images for hydrogen-to-oxygen ratios, H_2/O_2, of 6/1 and 2/1, respectively, in which each diffraction ring corresponds to a specific crystal plane. It is shown that, under $H_2/O_2 = 6/1$, there exist five distinct crystal planes: Cu_2O (111), Cu_2O (220), Cu (111), Cu (200), and Cu (220). When H_2/O_2 decreases to 2/1, the diffraction ring of Cu (200) disappears (as in Figure 2b) and the intensity of Cu (111) decreases. This suggests that the fraction of Cu will reduce greatly as hydrogen decreases in the reactants. Figure S8 (Supporting Information) illustrates the differences in diffraction peak intensities of different crystal facets under various H_2/O_2. As the hydrogen content in the reaction system increases, the diffraction intensity of the Cu crystal facets rises, while the diffraction intensity of the Cu_2O crystal facets decreases. This observation supports the general conclusion that hydrogen facilitates the reduction of oxides. Consequently, we have confirmed the identification of crystal facets associated with different diffraction peaks and validated that the SAED method is effective for phase differentiation.

As shown in Supporting Videos, most of the copper nanoparticles remain static under $H_2/O_2 = 2/1$. As H_2/O_2 increases to 6/1, the migration of copper nanoparticles becomes more pronounced. Hence, we first investigated the evolution of phase distribution on the surface of copper nanoparticles under reaction temperature $T = 500$ °C and $H_2/O_2 = 6/1$. Figure 2d illustrates that the intensity of different diffraction peaks varies periodically over the reaction time, indicating a continuous competition and oscillation between oxidation and reduction reactions. This oscillation between the two reactions leads to the ongoing conversion between Cu and Cu_2O, which is the main cause of the sustained driving force. As depicted in Figures 2c,d, and Figure S2 (Supporting Information), we can quantify the phase distribution over the copper nanoparticles surface during the migration process via a radial profile of the diffraction patterns. The

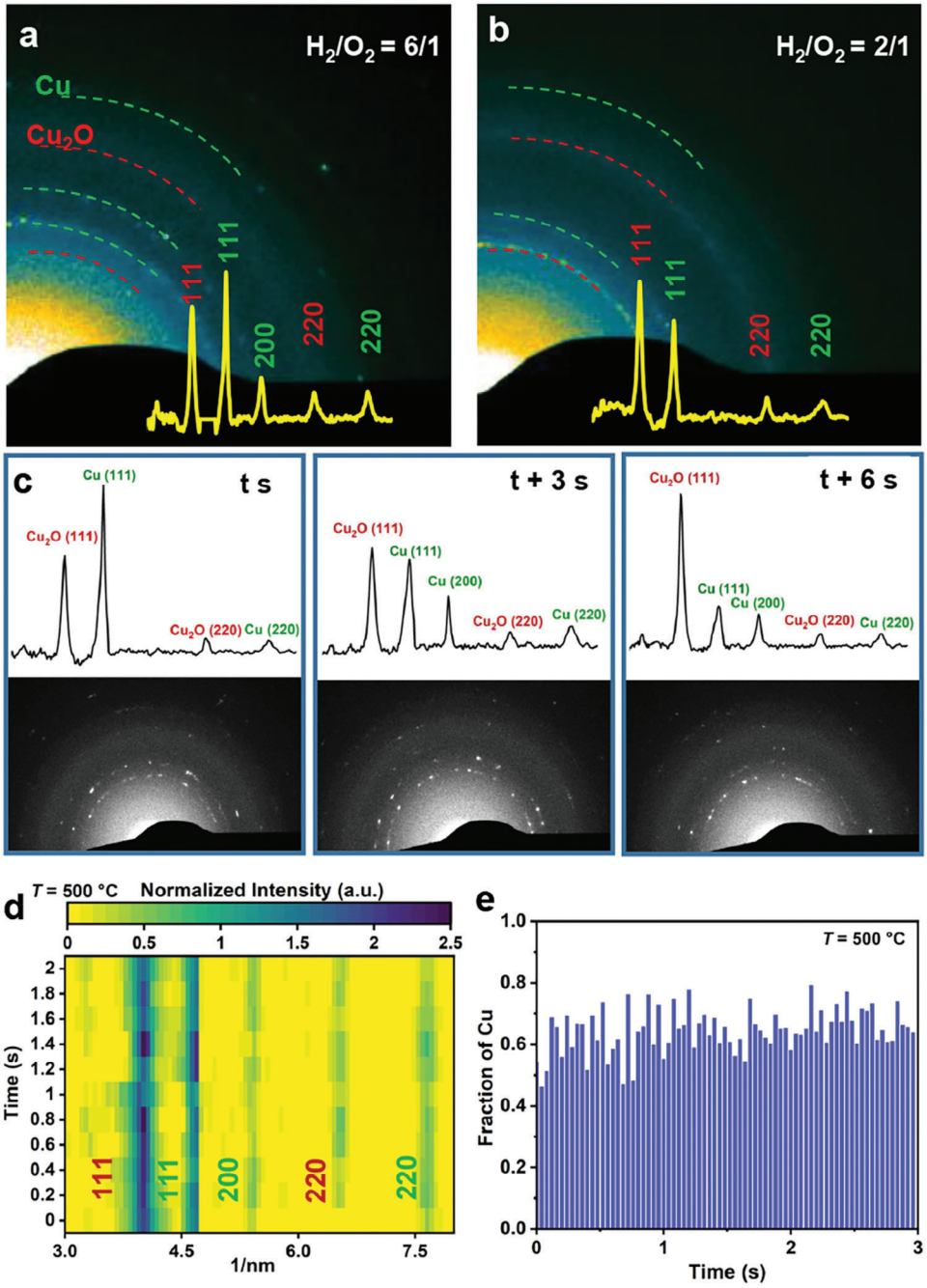

Figure 2. a,b) SAED images for H_2/O_2 = 6/1 and H_2/O_2 = 2/1. c,d) In situ SAED images and corresponding radial profiles during the redox reaction with T = 500 °C and H_2/O_2 = 6/1. e) Fraction of Cu phase during the redox reaction with T = 500 °C and H_2/O_2 = 6/1.

intensity of peaks associated with different crystal planes varies during the reaction. Of note, identical TEM imaging conditions were retained throughout the entire in situ experiment, which guaranteed the consistent background signals contributed by the electron scattering of amorphous SiNx membranes of reaction cells and therefore the reliability of phase quantification. Additionally, given that the number of particles within the field of view is sufficiently large and the volume of Cu nanoparticles is relatively small, we can safely disregard the oscillation effect of diffraction. The intensity of the diffraction peak corresponding to Cu or Cu_2O can be regarded as proportional to their respective volumes. We defined the fraction of the Cu phase on the surface of nanoparticles by dividing the sum of the intensities of Cu (111), Cu (200) peaks by the sum of the intensities of Cu_2O (111), Cu (111), and Cu (200) peaks, considering that these three peaks have remarkable changes during the reaction. Figure 2e shows that the fraction of the Cu phase oscillates during the reaction which is consistent as shown in Figure 2d, implying that the

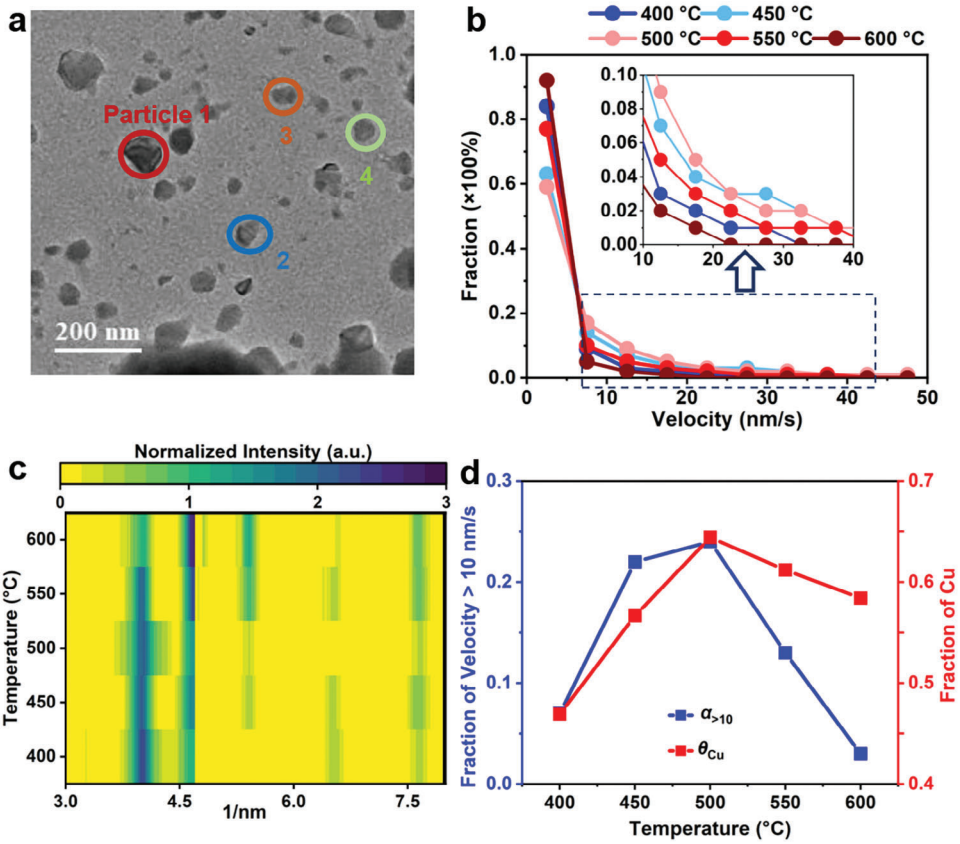

Figure 3. a) A typical TEM image of nano-copper particles utilized for image recognition. b) The velocity distribution of migrating nanoparticles at various temperatures with $H_2/O_2 = 6/1$ (by counting ≈6000 particles). The distribution of migrating nanoparticles within a velocity of 10 to 40 nm s^{-1} is illustrated in the embedded graph. c) Radial profiles of SAED patterns at t = 1s under various temperatures. d) The fraction of migrating velocity of nanoparticles exceeding 10 nm s^{-1} and the average fraction of Cu phase on the nanoparticles under various temperatures.

migration of copper nanoparticles is closely related to the competition between oxidation and reduction reaction. In detail, the fraction of the Cu phase oscillates ≈0.6, reflecting that there exists a long-term equilibrium of oxidation and reduction reaction though at a specific instance, the consumption rates of H_2 and O_2 may not be exactly balanced.

Nevertheless, the driving force model could allow us to qualitatively estimate the magnitude of the driving force acting on the copper nanoparticle during the migration once we obtained quantitative data on the fraction of the Cu phase on the nanoparticle surface.

2.3. Effects of Reaction Temperature on the Driving Force

To further understand the interplay between the reaction and the migration of copper nanoparticles, we conducted experiments at varying temperatures with fixed H_2/O_2 of 6/1. We first visualized the motion of copper nanoparticles via TEM images (see Videos S1–S5, Supporting Information). Using image recognition technology, we obtained the migration rates of particles from successive TEM images with a time step of 0.04 s. Subsequently, we classified the normalized migration velocities[42] of ≈6000 nanoparticles for different time intervals, and obtained velocity distribution as shown in **Figure 3**b. Additionally, Figure S3 (Supporting Information) shows the distribution of particle migration velocities at different temperatures. From Figure 3b and Figure S3 (Supporting Information), it is evident that at $T = 500$ °C, the fraction of particles within higher migration velocity becomes larger. We further analyzed the total fraction of particles with velocities higher than 10 nm s^{-1} (Figure 3d), which shows a trend of initial increase followed by a subsequent decrease, passing a maximum, as temperature increases.

The driving force model, as will be shown in the following, can be used to explain the observed trend of copper nanoparticle migration velocity with varying temperatures. Note that the reaction temperature will influence the driving force via k_1 and c_{Cu}, we simplified the proposed driving force model as:

$$\vec{F}\,\Delta t \approx \Delta t^2 P_{O_2} k_1 \overline{c_{Cu}} \tag{5}$$

The oxidation reaction of Cu involves four complex steps: the adsorption and desorption of oxygen, the breaking of O—O bonds, and the formation of Cu—O bonds. Since the step concerning the bond breaking is endothermic and meanwhile the step involving the bond formation is essentially exothermic, the effect of temperature on k_1 can be considered negligible.

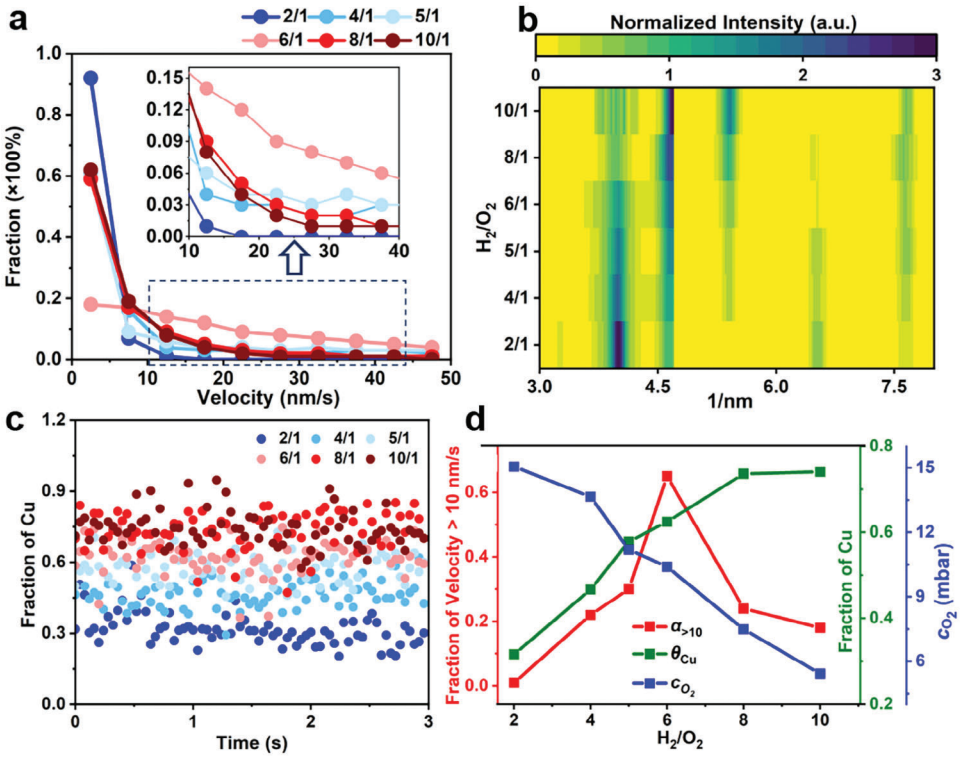

Figure 4. a) Distribution of migrating velocity of nanoparticles for various H_2/O_2 at $T = 500$ °C. The distribution of the migrating velocity of nanoparticles of 10 to 40 nm s^{-1} is illustrated in the embedded graph. b) Radial profiles of SAED patterns at t = 1s under various H_2/O_2. c) The evolution of the fraction of Cu phase under various H_2/O_2. d) The fraction of migrating velocity of nanoparticles exceeding 10 nm s^{-1} and the average fraction of Cu phase on the nanoparticles under various H_2/O_2.

We qualitatively compared the fraction of Cu phase on the surface of nanoparticles at different temperatures by use of the SAED patterns depicted in Figure 2. Figure 3c and Figure S4 (Supporting Information) illustrate the radial profiles of SAED patterns for different temperatures. From Figure 3c we observed that, as the temperature increases, the peak intensities corresponding to both Cu (111) and Cu (200) increase, and meanwhile the peak intensity corresponding to Cu_2O (111) decreases. As indicated by the Arrhenius equation, differences in activation energies result in different rates of change in reaction rate constants with temperature. Therefore, the contrasting trends observed in the two phases with temperature are attributable to the differences in activation energies between the oxidation and reduction reactions. Note that the peak intensity is closely related to the corresponding fractions of Cu phase on the surface of nanoparticles, in Figures S5,S6 (Supporting Information) we showed the fraction of Cu phase for different temperatures. In Figure 3d the average fraction of Cu phase within 0–3 s for each reaction temperature (Figure 3d) is also depicted. As can be seen, the fraction of the Cu phase reaches its maximum at $T = 500$ °C. Based on Equation (5), we can argue that there are consistent trends between the fractions of the Cu phase and the migration velocities of nanoparticles with a varying temperature. This also demonstrates that the driving force is directly relevant to the fraction of the Cu phase on the surface of the nanoparticle.

2.4. Effects of H_2/O_2 on the Driving Force

In the realm of the catalytic system, the gas composition exerts a pronounced influence on the redox reaction. Practically, we can manipulate the gas composition by adjusting the hydrogen or oxygen inlet flow rates. We established an environment comprising 80% helium and 20% reaction gases and regulated the gas composition within the system by modulating the flow rates of hydrogen and oxygen. We acquired a series of TEM images of copper nanoparticles under various H_2/O_2. By use of an image recognition algorithm, we tracked the migration trajectories of each particle and obtained migration velocities. Figure S7 (Supporting Information) illustrates the histogram of particle migration velocity, which reaches the maximum at $H_2/O_2 = 6/1$ (**Figure** 4a). We further conducted a statistical analysis to determine the fraction of migration velocity of nanoparticles exceeding 10 nm s^{-1} under different H_2/O_2 (Figure 4d). It shows that the migration velocity initially increases and then decreases as H_2/O_2 increases.

We further utilized the model to qualitatively understand the effect of H_2/O_2 on driving force. It shows that the driving force model can be rewritten as:

$$\vec{F}\Delta t \approx RT\Delta t^2 k_1 \overline{c_{O_2} c_{Cu}} \quad (6)$$

We compared the radial profiles of SAED patterns under different H_2/O_2, as depicted in Figures S8 (Supporting Information) and Figure 4b. As discussed above, the sum of the intensity of Cu (111) and Cu (200) is proportional to the fraction of Cu phase on the nanoparticles. The fraction of the Cu phase under different H_2/O_2 is illustrated in Figure S9 (Supporting Information) and Figure 4c. In Figure 4d, we showed the fraction of Cu phase averaged over 0–3 s for different H_2/O_2. We meanwhile collected the partial pressures of oxygen under different H_2/O_2 which are also presented in Figure 4d. It demonstrates that, as H_2/O_2 increases, the fraction of the Cu phase on the nanoparticle surface increases. This can be attributed to the enhanced reduction of the Cu_2O phase in a hydrogen-rich atmosphere. The faction of Cu phase, c_{Cu}, and the concentration of oxygen, c_{O2}, which influence the driving force as determined through our model analysis, respectively exhibit a monotonic increase and a monotonic decrease with the increase of H_2/O_2. Concurrently, experimental measurements of migration velocity show a trend of initially increasing and then decreasing with a peak at $H_2/O_2 = 6/1$. The trend is related to the dynamic balance between oxidation and reduction reactions. Specifically, we noted that since oxidation and reduction reactions are in dynamic equilibrium, any limitation on either reaction will impact the overall catalytic process. At lower H_2/O_2 with excessive c_{O2}, the reduction reaction of Cu_2O will be hindered. At high H_2/O_2 and large concentrations of hydrogen, c_{Cu} is substantial, but the oxidation rate of Cu is low due to the limited oxygen concentration. As the H_2/O_2 increases, the previously limited reduction reaction gradually regains effectiveness, and thus the oscillation between oxidation and reduction reactions intensifies, leading to an increase in the driving force of particle migration. However, with further increases in the H_2/O_2, the oxidation reaction becomes progressively constrained, leading to a lengthening of the oscillation cycle between oxidation and reduction reactions, and a corresponding decrease in the force driving particle migration. As a result, a maximal migration velocity could be reached. The competition between hydrogen and oxygen ratio would constrain the overall catalytic reaction. Suppose the partial pressure of oxygen increases, which would lead to a change in gas composition (i.e., the H_2/O_2), the migration velocity is expected to first decrease and then increase. If the H_2/O_2 remains constant while the total pressure of the reaction system continues to increase, the driving force will also increase due to the corresponding rise in $c_{O2}RT$. In this study, we did not analyze additional influencing parameters. By analyzing the peak driving force, we can identify the conditions under which the catalytic reaction is most intense. This allows us to adjust particle migration velocities by controlling the chemical environment, providing an effective approach to regulating the sintering of metal nanoparticles.

3. Conclusion

In this study, we systematically investigated the migration dynamics of nano-copper particles during redox reactions through in situ HRTEM methodology. Realtime high-resolution evidence shows that the asymmetric distribution of Cu and Cu_2O phases on the surface of migrating nano-copper particles during catalytic reactions, resulting from the competition between oxidation and reduction reaction rates, is closely related to nanoparticle migration. Specifically, the reduction and oxidation near the surface areas filled with, respectively, Cu and Cu_2O phases, could facilitate the pressure gradient around the particle which drives the migration of nano-particles.

A close analysis of the interplay between chemical reactions and particle migration velocities suggests that a driving force model for particle migration, which relates the migration velocity directly to the rate constants of chemical reactions k_1, reaction temperature T, average oxygen concentration c_{O2}, and the concentration of copper $c_{Cu,}$ can be established and used to qualitatively compare the magnitude of the driving force under different reaction conditions.

We further examined the particle migration under various temperatures and hydrogen-to-oxygen ratio H_2/O_2. We observed that, by increasing temperature from 400 to 600 °C, the migration velocity first increases and then decreases, reaching a maximum at a temperature of 500 °C. A similar maximum migration velocity was also found at the $H_2/O_2 = 6/1$ when H_2/O_2 changes from 2/1 to 10/1. By using the model, we could understand the trend of the driving force with increasing temperature and H_2/O_2. This shows that the model can qualitatively capture the physics of driving forces and thus migration under different reaction conditions. We expect this work can add a potential yet critical perspective to understand particle migration and thus the nano-metal catalyst particle sintering in heterogeneous catalysis.

Supporting Information

Supporting Information is available from the Wiley Online Library or from the author.

Acknowledgements

The authors thank the financial support from the National Natural Science Foundation of China (Grant Nos. 22293021). The in situ atmosphere microscopy study in this work was supported by the project of DICP-DENS Laboratory for In Situ Microscopy Applications.

Conflict of Interest

The authors declare no conflict of interest.

Data Availability Statement

The data that support the findings of this study are available from the corresponding author upon reasonable request.

Keywords

driving force model, electron microscopy, in situ technique, nano-copper migration, nanoparticles

Received: July 10, 2024
Revised: August 22, 2024
Published online: September 2, 2024

[1] K. Bae, D. Y. Jang, H. J. Choi, D. Kim, J. Hong, B. K. Kim, J. H. Lee, J. W. Son, J. H. Shim, *Nat. Commun.* **2017**, *8*, 14553.

[2] A. A. Gokhale, J. A. Dumesic, M. Mavrikakis, *J. Am. Chem. Soc. B* **2008**, *130*, 1402.
[3] H. Bluhm, M. Hävecker, A. Knop-Gericke, E. Kleimenov, R. Schlögl, D. Teschner, V. I. Bukhtiyarov, D. F. Ogletree, M. Salmeron, *J. Phys. Chem. B* **2004**, *108*, 14340.
[4] D. Gao, R. M. Arán-Ais, H. S. Jeon, B. R. Cuenya, *Nat. Catal.* **2019**, *2*, 198.
[5] J. Lu, B. Fu, M. C. Kung, G. Xiao, J. W. Elam, H. H. Kung, P. C. Stair, *Science* **2012**, *335*, 1205.
[6] S. R. Challa, A. T. Delariva, T. W. Hansen, S. Helveg, J. Sehested, P. L. Hansen, F. Garzon, A. K. Datye, *J. Am. Chem. Soc.* **2011**, *133*, 20672.
[7] H. Chen, S.-Z. Yang, Z. Yang, W. Lin, H. Xu, Q. Wan, X. Suo, T. Wang, D.-e. Jiang, J. Fu, S. Dai, *ACS Cent. Sci.* **2020**, *6*, 1617.
[8] S. L. Scott, *ACS Catal.* **2018**, *8*, 8597.
[9] P. Yin, S. Hu, K. Qian, Z. Wei, L.-L. Zhang, Y. Lin, W. Huang, H. Xiong, W.-X. Li, H.-W. Liang, *Nat. Commun.* **2021**, *12*, 4865.
[10] E. M. Dietze, F. Abild-Pedersen, P. N. Plessow, *J. Phys. Chem. C* **2018**, *122*, 26563.
[11] L. Wang, S. Xu, S. He, F.-S. Xiao, *Nano Today* **2018**, *20*, 74.
[12] S. H. Joo, J. Y. Park, C.-K. Tsung, Y. Yamada, P. Yang, G. A. Somorjai, *Nat. Mater.* **2009**, *8*, 126.
[13] U. Aslam, V. G. Rao, S. Chavez, S. Linic, *Nat. Catal.* **2018**, *1*, 656.
[14] G. Prieto, J. Zečević, H. Friedrich, K. P. de Jong, P. E. de Jongh, *Nat. Mater.* **2013**, *12*, 34.
[15] Z. Li, N. M. Schweitzer, A. B. League, V. Bernales, A. W. Peters, A. B. Getsoian, T. C. Wang, J. T. Miller, A. Vjunov, J. L. Fulton, J. A. Lercher, C. J. Cramer, L. Gagliardi, J. T. Hupp, O. K. Farha, *J. Am. Chem. Soc.* **2016**, *138*, 1977.
[16] H. Tang, Y. Su, B. Zhang, A. F. Lee, M. A. Isaacs, K. Wilson, L. Li, Y. Ren, J. Huang, M. Haruta, B. Qiao, X. Liu, C. Jin, D. Su, J. Wang, T. Zhang, *Sci. Adv.* **2017**, *3*, 1700231.
[17] H. Frey, A. Beck, X. Huang, J. A. van Bokhoven, M. G. Willinger, *Science* **2022**, *376*, 982.
[18] A. Beck, X. Huang, L. Artiglia, M. Zabilskiy, X. Wang, P. Rzepka, D. Palagin, M. G. Willinger, J. A. van Bokhoven, *Nat. Commun.* **2020**, *11*, 3220.
[19] S. Hu, W.-X. Li, *Science* **2021**, *374*, 1360.
[20] Y.-R. Wang, Q. Zhuang, R. Cao, Y. Li, F.-Y. Gao, Z.-R. Li, Z. He, L. Shi, Y.-F. Meng, X. Li, J.-L. Wang, Y. Duan, M.-R. Gao, X. Zheng, S.-H. Yu, *Nano Lett.* **2022**, *22*, 4232.
[21] S. Zhang, L. Nguyen, Y. Zhu, S. Zhan, C.-K. Tsung, F. Tao, *Acc. Chem. Res.* **2013**, *46*, 1731.
[22] F. Tao, P. A. Crozier, *Chem. Rev.* **2016**, *116*, 3487.
[23] X. Huang, T. Jones, A. Fedorov, R. Farra, C. Coperet, R. Schlogl, M. G. Willinger, *Adv. Mater.* **2021**, *33*, 2101772.
[24] H. Werner, D. Herein, G. Schulz, U. Wild, R. Schlögl, *Catal. Lett.* **1997**, *49*, 109.
[25] G. Zhou, L. Luo, L. Li, J. Ciston, E. A. Stach, W. A. Saidi, J. C. Yang, *Chem. Comm.* **2013**, *49*, 10862.
[26] R. H. Milne, A. Howie, *Philos. Mag. A* **2006**, *49*, 665.
[27] L. Luo, Y. Kang, J. C. Yang, G. Zhou, *Surf. Sci.* **2012**, *606*, 1790.
[28] A. P. LaGrow, M. R. Ward, D. C. Lloyd, P. L. Gai, E. D. Boyes, *J. Am. Chem. Soc.* **2017**, *139*, 179.
[29] E. Ruska, *Kolloid-Zeitschrift* **1942**, *100*, 212.
[30] P. L. Hansen, J. B. Wagner, S. Helveg, J. R. Rostrup-Nielsen, B. S. Clausen, H. Topsøe, *Science* **2002**, *295*, 2053.
[31] W. Yuan, D. Zhang, Y. Ou, K. Fang, B. Zhu, H. Yang, T. W. Hansen, J. B. Wagner, Z. Zhang, Y. Gao, Y. Wang, *Angew. Chem. Int. Ed.* **2018**, *57*, 16827.
[32] X. Zhang, S. Han, B. Zhu, G. Zhang, X. Li, Y. Gao, Z. Wu, B. Yang, Y. Liu, W. Baaziz, O. Ersen, M. Gu, J. T. Miller, W. Liu, *Nat. Catal.* **2020**, *3*, 411.
[33] M. Tang, W. Yuan, Y. Ou, G. Li, R. You, S. Li, H. Yang, Z. Zhang, Y. Wang, *ACS Catal.* **2020**, *10*, 14419.
[34] Q. Zhang, J. Ma, L. Mei, J. Liu, Z. Li, J. Li, Z. Zeng, *Matter* **2022**, *5*, 1235.
[35] J. Zhang, Z. Sun, Z. Kang, H. Lin, H. Liu, Y. He, Z. Zeng, Q. Zhang, *Adv. Funct. Mater.* **2022**, *32*, 2204976.
[36] R. Yang, L. Mei, Z. Lin, Y. Fan, J. Lim, J. Guo, Y. Liu, H. S. Shin, D. Voiry, Q. Lu, J. Li, Z. Zeng, *Nat. Rev. Chem* **2024**, *8*, 410.
[37] L. Zhou, Y. Sun, Y. Wu, Y. Zhu, Y. Xu, J. Jia, F. Wang, R. Wang, *Nano Lett.* **2023**, *23*, 11360.
[38] H. Zhao, Y. Zhu, H. Ye, Y. He, H. Li, Y. Sun, F. Yang, R. Wang, *Adv. Mater* **2023**, *35*, 2206911.
[39] Y. Zhu, Z. Zhao, Y. Xu, R. Wang, *Small Methods* **2024**, 2400179.
[40] A. J. Wilkinson, P. B. Hirsch, *Micron* **1997**, *28*, 279.
[41] J. Yu, W. Yuan, H. Yang, Q. Xu, Y. Wang, Z. Zhang, *Angew. Chem. Int. Ed.* **2018**, *57*, 11344.
[42] D. Gao, X. Li, B. Hou, F. Lu, M. Ye, A. Wang, X. Wang, *Chem. Eng. Sci.* **2022**, *252*, 117532.